Microchimica Acta (2024) 191:617
https://doi.org/10.1007/s00604-024-06644-2

RESEARCH

Sensitive and reliable lab-on-paper biosensor for label-free detection of exosomes by electrochemical impedance spectroscopy

Sevda Akay Sazaklioglu[1,2] · Hilal Torul[3] · Uğur Tamer[3,4] · Hilal Kabadayi Ensarioglu[5] · Hafize Seda Vatansever[5,6] · Bilal H. Gumus[7] · Hüseyin Çelikkan[8]

Received: 10 July 2024 / Accepted: 19 August 2024
© The Author(s), under exclusive licence to Springer-Verlag GmbH Austria, part of Springer Nature 2024

Abstract

A new, sensitive, and cost-effective lab-on-paper-based immunosensor was designed based on electrochemical impedance spectroscopy (EIS) for the detection of exosomes. EIS was selected as the determination method since there was a surface blockage in electron transfer by binding the exosomes to the transducer. Briefly, the carbon working electrode (WE) on the paper electrode (PE) was modified with gold particles (AuPs@PE) and then conjugated with anti-CD9 (Anti-CD9/AuPs@PE) for the detection of exosomes. Variables involved in the biosensor design were optimized with the univariate mode. The developed method presents the limit of detection of 8.7×10^2 exosomes mL^{-1}, which is lower than that of many other available methods under the best conditions. The biosensor was also tested with urine samples from cancer patients with high recoveries. Due to this a unique, low-cost, biodegradable technology is presented that can directly measure exosomes without labeling them for early cancer or metastasis detection.

Keywords Paper-based electrode · Gold particle modified electrode · Exosomes · Electrochemical impedance spectroscopy · Label-free detection

Introduction

Cancer, known to have more than 100 types, has the highest mortality rate in modern times, despite the opportunities for early diagnosis and personal treatment [1]. Determining tumors at an early stage is a vital component of cancer control, which is possible by detecting the correct cancer markers in various forms such as DNA, miRNA, and proteins in the tumor tissue or serum [2, 3]. Recently, exosomes, one of the extracellular vesicles, have emerged as an alternative mediator of cell-to-cell communication in the tumor microenvironment and cancer metastasis, leading to the

Highlights

- Impedimetric detection of exosomes with paper electrodes has been suggested for early cancer detection.
- Simple, rapid, real-time quantitative determination of exosomes takes only 40 min.
- The lowest LOD for exosomes in PBS medium was 8.7×10^2 exosomes mL^{-1}.
- The biosensor design allowed analysis in a sample volume as low as 5 µL.
- Exosomes in urine samples taken from patients were detected with 79% to 110% recoveries.

✉ Hüseyin Çelikkan
celikkan@gazi.edu.tr

[1] Faculty of Pharmacy, Department of Analytical Chemistry, Ankara Medipol University, 06050 Ankara, Turkey

[2] Graduate School of Natural and Applied Science, Gazi University, 06560 Ankara, Turkey

[3] Faculty of Pharmacy, Department of Analytical Chemistry, Gazi University, 06330 Ankara, Turkey

[4] METU MEMS Center, Ankara, Turkey

[5] Faculty of Medicine, Department of Histology and Embryology, Manisa Celal Bayar University, 45200 Manisa, Turkey

[6] DESAM Institute, Near East University, Mersin 10, Turkey

[7] Faculty of Medicine, Department of Urology, Manisa Celal Bayar University, 45200 Manisa, Turkey

[8] Faculty of Science, Department of Chemistry, Gazi University, 06560 Ankara, Turkey

Published online: 24 September 2024

intracellular transfer of information from donor cells to recipient cells the direct uptake or release of extracellular signaling molecules [4]. First, tumor-derived exosomes' ability to transfer miRNAs from metastatic to less metastatic cells facilitates tumor growth and metastasis [5, 6]. In addition, exosomes which contain bioactive molecules produced by cancer cells can stimulate the immune response. Studies show that the level of exosomes in the body fluids such as urine and plasma of cancer patients is significantly higher than in healthy individuals [7–9]. For this reason, many researchers hypothesize that exosome levels in body fluid may serve as a diagnostic biomarker in cancer patients [10–13]. Due to the proteins on their surfaces, the determination of exosomes can be performed by Enzyme-Linked Immunosorbent Assay (ELISA) and Western Blot (WB). However, these methods are unsuitable for routine clinical analysis because they require large sample volumes, are difficult to handle, and need specialized instrumentation. On the other hand, biosensors are generally considered good candidates for such applications as they are sensitive, selective, reliable, and low-cost. Therefore, exosome biosensors have been developed using many optical, electrochemical, and colorimetric methods [14–18].

The membranes of exosomes contain an abundance of tetraspanins that are specific to endosomes, including CD9, CD63, and CD81 [19]. These proteins play a crucial role in orchestrating diverse molecular interactions, amplifying their functions, and governing various cellular processes including cell adhesion, motility, growth, differentiation, and signal transduction [20]. Notably, the CD9 antigen is part of the tetraspanin family. CD9 is a protein involved in cell signaling and adhesion. It is found on the surface of various cells, including cancer cells, and plays a role in the communication between cancer cells and their microenvironment [21]. In cancer patients, the expression of the exosomal markers (CD63 and CD9) is higher in malignant cells compared to adjacent normal cells [22, 23]. To target them, several biosensors have been developed, showing interesting diagnostic tools in the early stages of cancer [24–26].

The most important challenges in designing exosome biosensors are their small size and low concentration in body fluids. Electrochemical biosensors have become an ideal option for exosome detection due to their high sensitivity, low sample requirement, and easy instrumentation [27]. The electrochemical biosensor converts the identification information of biomolecules into potential, current, and impedance electrochemical signals [28]. The significance of EIS compared to other electrochemical techniques lies in its ability to differentiate and offer extensive information on various electrical, electrochemical, and physical processes occurring in a real electrochemical system [29]. Moreover, EIS can be performed as a label-free detection method promising the potential to facilitate rapid tests [30–34]. The impedimetric response of an exosome, Z, consists of the real (passive element) part, Z_r, and the imaginary (active element) part, Z_i. This impedance is a measure of the exosome's ability to resist electron current flow and depends on its shape, size, and dielectric properties [35]. Therefore, this electrochemical method is widely used to investigate different molecular interactions, especially in immunosensors [36, 37].

An ideal biosensor should meet real applications' low-cost and stability requirements. Paper-based analytical devices (PADs) have recently received much attention as an effective way to develop miniature and lightweight devices at a low cost. Paper electrodes, in which the recognition components such as enzymes, antibodies, and aptamers can be easily immobilized [38–40], can meet the needs of both medical laboratory investigations and point-of-care-testing (POCT) applications [41–44]. This naturally occurring and sustainable material can undergo processing techniques similar to those used in microfluidic-based diagnostics. As the liquid can pass through the porous substrate via capillary action, the necessity for pumping systems is eliminated, and only small sample volumes are necessary. Additionally, printed paper featuring hydrophilic channels bordered by hydrophobic walls enables the distribution of samples into distinct spatial regions, facilitating the simultaneous execution of multiple assays on a single device [45, 46].

Herein, we developed an electrochemical paper-based biosensor for the selective and sensitive detection of exosomes by improving the models we designed before [26, 47]. To our knowledge, for the first time, an AuPs-modified paper electrode system (AuPs@PE) was developed and applied here for impedimetric detection of exosomes. Moreover, the advantages of this paper-based immunosensor, such as being portable and disposable, make it superior. First, we focused on gold nanostructures including a large surface area-to-volume ratio, unique optical and electronic characteristics, and the ability to be easily functionalized for the adsorption of various biomolecules [48, 49]. Since exosomes contain CD9 surface antigens, Au-accumulated PEs were conjugated with anti-CD9 antibodies for the biosensor system. Then, the Anti-CD9/AuPs@PEs interacted with different concentrations of exosomes. In the presence of a $[Fe(CN)_6]^{3-/4-}$ redox system as a faradaic probe, RCT resulting from the binding of biomolecules was observed. The RCT response after exosome binding corresponds to the number of captured exosomes and serves as a proof-of-concept to detect and quantify cancer cell-derived exosomes. In addition, the developed system was tested both in a PBS environment and urine samples collected from healthy and prostate cancer patients.

Experiments

Chemicals and reagents

Lyophilized PC-3 (human metastatic prostate cancer cell line) Exosome Standard (ab239689) was purchased from Abcam, UK. CD9 (C-4) monoclonal antibody was purchased from Santa Cruz Biotechnology, Inc., and it was used without further purification and diluted in PBS 7.4. The number of exosomes in urine samples was determined with the EXEL-ULTRA-CD63-1 kit purchased from System Biosciences. Nitrocellulose (NC) membrane (FF80HP, 210 × 297 mm) was purchased from Whatman, Cytiva, Marlborough, MA, USA. Conductive carbon paste (DS-7452CB) was supplied from Daejoo Electronic Materials (Shanghai, South Korea). Silver chloride ink was purchased from Gwent Group (Torfaen, UK). Tetrachloroauric(III) acid ($HAuCl_4$) was purchased from BDH Ltd, Poole, England. Other chemicals were supplied from Sigma, St. Louis, MO, and Merck (Vienna, Austria) (see supporting information for details).

Instrument

All electrochemical measurements were carried out using IVIUM-CompactStat potentiostat. Processing of impedance measurements was performed by ZsimpWin 3.22 software, and RCT was calculated using suitable equivalent circuits. The exosome number of samples was determined at 450 nm using the NanoDrop ND-1000 spectrophotometer. XEROX ColorQube™ 8570 brand wax printer was used to design barrier circles on the paper-based electrodes.

Urine sample collection

For exosome analysis, 5.0 mL of urine samples were taken from each patient in all groups. Urine samples from all patients were centrifuged at 4000 rpm for 20 min. The supernatant was collected and stored at − 80 °C until the next use. All processes were carried out according to the experimental application plan and collection norms. The details of ethical procedures are presented in the supporting information.

The groups belonging to the study are as follows:

Group I: Patients in the control group who do not have prostate problems and who applied to the clinic for urinary reasons.
Group II: Patients diagnosed with prostatitis and undergoing biopsy.
Group III: Patients diagnosed with prostate cancer for the first time but not treated. Both patients had a Gleason score (3 + 3) of 6/10.

Exosomes were obtained from the urine samples of Group 1, Group 2, and Group 3 patients with the Qiagen-HB-2436 Kit. Then, the exosome quantification was performed with the ELISA kit (EXEL-ULTRA-CD63-1). The standard amount of exosome in the Biovision TumorExoRNATM (K1231-20) kit was used as a positive control. The calibration curve of the measurements obtained from the standards is presented in Figure S1.

As a result, the groups of exosomes in urine samples were categorized by the diagnosis types. In addition, the letter "G" indicates the group number, and the letter "P" indicates the patient number.

Characterization of the standard and urine exosomes by high contrast transmission electron microscopy (CTEM)

Exosomes were fixed by preparing a 1% glutaraldehyde solution and then incubated for 10 min. A 5 µL of exosome sample was adsorbed on 200-mesh copper grids coated with formvar-carbon. The excess solution was removed with filter paper after 5 min. The grid was briefly placed on 10 µL of 2% uranyl acetate (saturated) solution for negative staining. After 1-min incubation, the step was repeated for washing with distilled water and left to dry overnight. The grids were then observed using FEI Tecnai G^2 Spirit BioTwin CTEM.

Fabrication of paper-based electrodes

Whatman FF80HP Membranes were used as paper material. A design to facilitate working on paper-based electrodes was performed. First, double barriers with 3-mm and 10-mm diameters were created on the membrane surface using wax printing. While the 10-mm diameter barrier consists of working, reference, and counter electrodes, the 3-mm barrier includes only the working electrode. Then, a 1-mm-thick steel mask was employed to set up the three-electrode system on the NC membrane. For this purpose, this mask was placed on a paper electrode, and carbon ink was applied to create electrodes. Following this step, Ag/AgCl ink was applied additionally to form the reference electrode on the appropriate place of electrode design. It was then cured at 90 °C for 5 min to fix the carbon ink on the NC membrane surface, melt, and penetrate the wax into the NC membrane. Finally, copper tapes were attached to the connection part of the electrodes to facilitate the electrical connection. The whole fabrication process of the paper electrodes, an image of printed PEs, and performing EIS measurement are shown in Figure S2.

Au accumulation on the working electrode

To decorate the paper electrodes with Au particle accumulation, 125.0 µL of 0.1 M KCl solution containing 5.0 mM chloroauric acid was added onto the paper electrode surface, and the electrodeposition of gold particles was achieved on the working electrode by applying − 0.3 V as constant potential during 600 s with the chronoamperometric method [50].

The conjugation of Anti-CD9 on AuPs modified paper electrodes

A 500.0 µL of 20.0 mM 11-mercaptoundecanoic acid (MUA) in EtOH/H_2O (8:1) solution was applied to the AuPs@PE and left in the dark to mix for 24 h. After the modification step, the electrodes were washed with 2.0 mL of EtOH to remove residuals. Then, 150.0 µL solution consisting of 0.4 M EDC and 0.1 M NHS was applied to each surface for 1 h to activate the carboxyl group of MUA. The electrodes were washed with 1.0 mL of distilled water. For the antibody conjugation of the surfaces, 5.0 µL of 4.0 ng μL^{-1} anti-CD9 was applied to the working electrode surface. Finally, Anti-CD9/AuPs@PE was washed with PBS (pH 7.4) and treated with % 0.1 bovine serum albumin to avoid non-specific bindings.

Characterization of the paper-based electrodes by scanning electron microscopy (SEM)

Scanning electron microscopy (SEM) images were obtained with QUANTA 400F Field Emission SEM. While the additional processing was not applied to record the SEM images of PE, AuPs@PE, and Anti-CD9/AuPs@PE, a treatment using glutaraldehyde was applied to the standard exosome-captured Anti-CD9/AuPs@PEs. For this purpose, firstly, 5.0 µL of 2.5% glutaraldehyde was applied to the electrode, then washed with ethanol for dehydration and left to dry [51]. Ultimately, the SEM image of the exosome (5.0 µL of 1.0×10^8 exosomes mL^{-1}) captured Anti-CD9/AuPs@PE was recorded. Four SEM images belong to separately prepared surfaces.

Exosome detection by EIS

EIS measurements were performed on a potential exhibiting faradaic condition through a sinusoidal potential perturbation with a frequency range of 1 to 10^5 Hz, with 26 data point readings and an amplitude of 0.01 V. EIS data was placed in a suitable equivalent circuit using ZsimpWin 3.22 software. The R(C(RW)), R(CR)W, and R(Q(RW)) equivalent circuit models are used to obtain RCT. These equivalent circuit models contain RS, CDL, RCT, CPE, and ZW components: These circuit elements indicate the resistance of the current passing through the solution, the charge transfer resistance, the double-layer capacitance formed between the surface and the liquid, constant phase element, and the 45° inclined diffusion resistance element, respectively. EIS measurements were performed with a three-electrode system consisting of a working electrode, a counter electrode, and a reference electrode. A 5.0 µL of standard exosome samples at different concentrations were applied to Anti-CD9/AuPs@PE, separately, and RCT values were recorded after 40 min of incubation. The voltage exhibiting faradaic condition in the impedance measurements was determined to be 0.1 V from the cyclic voltammogram taken before the measurement, and the impedance measurements of the prepared immune sensors were taken from 5.0 mM $[Fe(CN)_6]^{3-/4-}$ in 0.1 M KCl pH 7.4 solution.

Results and discussion

Characterization of the standard and urine exosomes by CTEM

The standard exosomes were validated by using CTEM. Exosomes were detected according to shape and edge contrast criteria. As seen in Figs. 1A and B, negative staining of exosome edges with uranyl acetate gave a better response in standard exosomes. Figure 1B showed that the exosomes are spherical vesicles with an average diameter of about 50 nm. In Fig. 1C, G3P1 coded urine sample, the exosome is lighter than the background in the complex sample environment. Standard exosomes were also slightly smaller than urine exosomes. Round-shaped morphologies of exosomes are seen clearly in all three images.

Characterization of the paper-based electrodes

Cyclic voltammetry (CV) was used to characterize PE and AuPs@PE. CV method was performed at a scan rate of 50 mV/s with sampling potentials ranging from − 1.0 to + 1.0 V. The current values (I_c and I_a) obtained after AuPs accumulation are considerably higher than those of unmodified PE (Fig. 2A). The anodic and cathodic peak currents of the modification stages are also shown in Table S1. This indicates that the accumulation of AuPs on the PE surface enhances electron transfer.

EIS measurements presented in Fig. 2B were performed to examine the changes in the charge transfer resistance (RCT) of both PE and AuPs@PE as working electrodes. While the charge transfer resistance of PE as the bare paper electrode was calculated to be 1625 ± 32 Ω (2.0% of RSD, $n = 3$), a significant decrease in the charge transfer

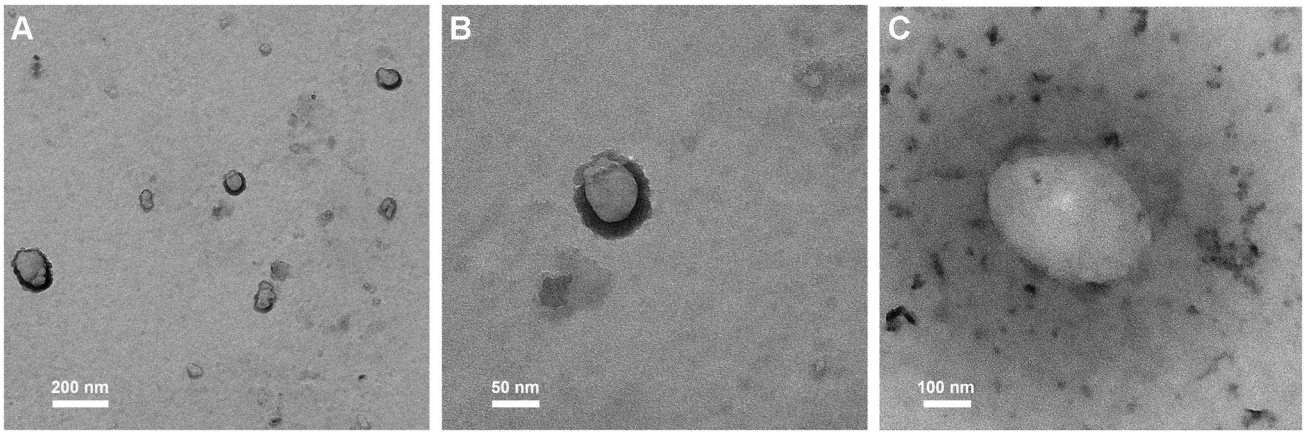


Fig. 1 CTEM of standard exosomes at different magnifications (**A**) and (**B**), and G3P1 urine exosomes (**C**)

resistance occurred after AuPs accumulation, and the RCT of AuPs@PE was obtained to be 227 ± 9 Ω (4% of RSD, $n = 3$). The results are shown in Table S2. A significant increase in RCT confirmed that electron transfer accelerated by coating AuPs on the carbon surface.

Scanning electron microscopy (SEM) was used to characterize the surfaces of the PE, AuPs@PE, Anti-CD9/AuPs@PE, and the exosomes on Anti-CD9/AuPs@PE, respectively. Figure 3A shows unmodified PE, i.e., only carbon paste-coated PE, while Fig. 3B shows the morphology, shape, and size of the AuPs accumulated on the PE surface by electrochemical reduction. The homogeneous decoration of AuPs on PE is clearly shown in Fig. 3B. We observed AuPs on PE as different sizes, sharp-edged, and localized particles. The decrease in the brightness of AuPs was caused by the antibody covering the surface and was indicated in Fig. 3C. Scanning electron micrograph of the exosomes with preserved membrane integrity revealed that the particles had a spherical shape and were approximately 50–100 nm in diameter. The image of exosomes shown with red arrows in Fig. 3D is compatible with the studies in the literature [52–54]. We have also included additional SEM images of exosome-capturing Anti-CD9/AuPs@PE to the supporting information in Figure S3.

SEM with energy dispersive X-ray spectroscopy (SEM/EDX), one of the most widely used surface characterization techniques, was also used in this study. Using the EDX method, the results including the chemical composition of a sample, their distribution, and concentration can be quickly generated. In addition to SEM images of PE and AuPs@PE, SEM–EDX analysis was performed to prove the formation of gold particles on the paper surface. As a result of the EDX analysis of PE indicated in Figure S4A, it is seen that the C and O atoms are dominant. After coating, Au atoms on the surface were observed for AuPs@PE (Figure S4B).

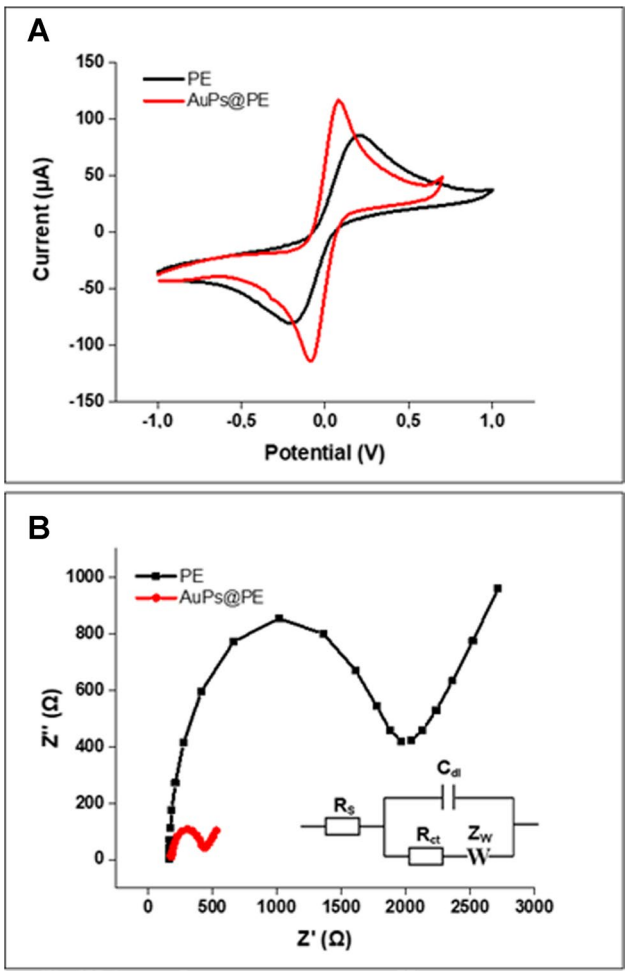


Fig. 2 CV (**A**) and EIS (**B**) measurements of PE and AuPs@PE, 5.0 mM $[Fe(CN)_6]^{3-/4-}$ in 0.1 M KCl pH 7.4 solution was used as electrolyte

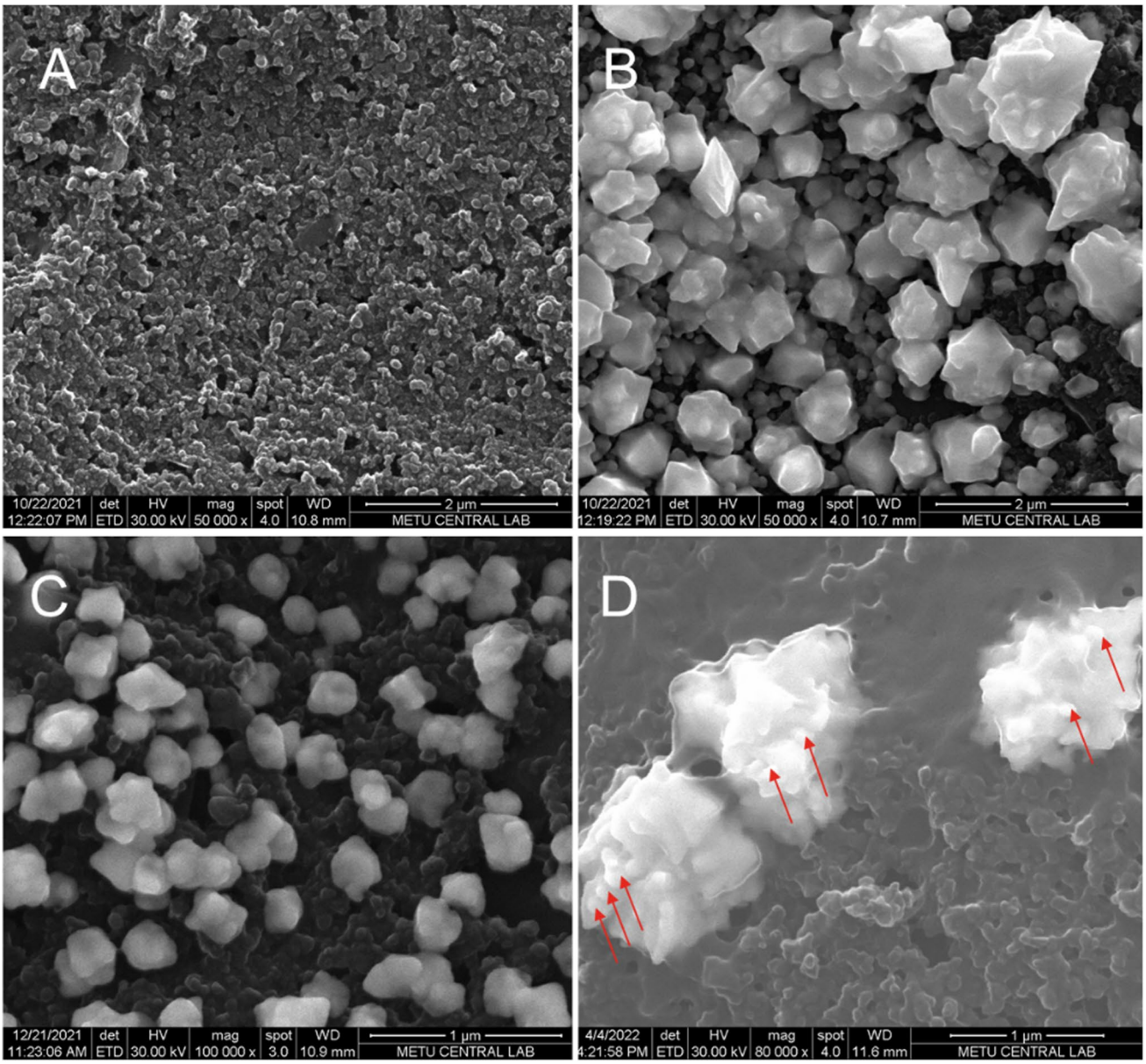


Fig. 3 SEM images of PE (**A**), AuPs@PE (**B**), Anti-CD9/AuPs@PE (**C**), and exosome-capturing Anti-CD9/AuPs@PE (**D**)

Optimization of the experimental conditions

The extent to which the experimental parameters affect the response of the exosome sensor was determined by the electrochemical impedance technique. The constant conditions of the optimization studies were 2 ng μL^{-1} of anti-CD9, 60 min of incubation time, and 25 °C of incubation temperature, and the response of Anti-CD9/AuPs@PE was measured against 1.0×10^{12} exosomes mL^{-1}. To ensure the selectivity and sensitivity of the exosome sensor, the effect of anti-CD9 concentration on the present was investigated. Figure 4A shows that the response RCT increases with the increase of the anti-CD9 concentration up to 4.0 ng μL^{-1}. Using 8.0 ng μL^{-1} of anti-CD9 did not enhance the RCT response. Therefore, the anti-CD9 concentration was optimized at 4.0 ng μL^{-1} to achieve high selectivity and sensitivity. The influence of the incubation temperature was studied at + 4, + 25, and + 37 °C. Since the maximum increase in RCT was observed at + 25 °C, this point was determined as the optimum incubation temperature as shown in Fig. 4B. The influence of the incubation time was studied in the 20–60-min range. If the incubation period is too long, non-specific adsorption may develop, and unexpected RCT values may occur. Based on Fig. 4C, the best binding period was found 40 min, regarding the highest RCT. Nyquist diagrams obtained in

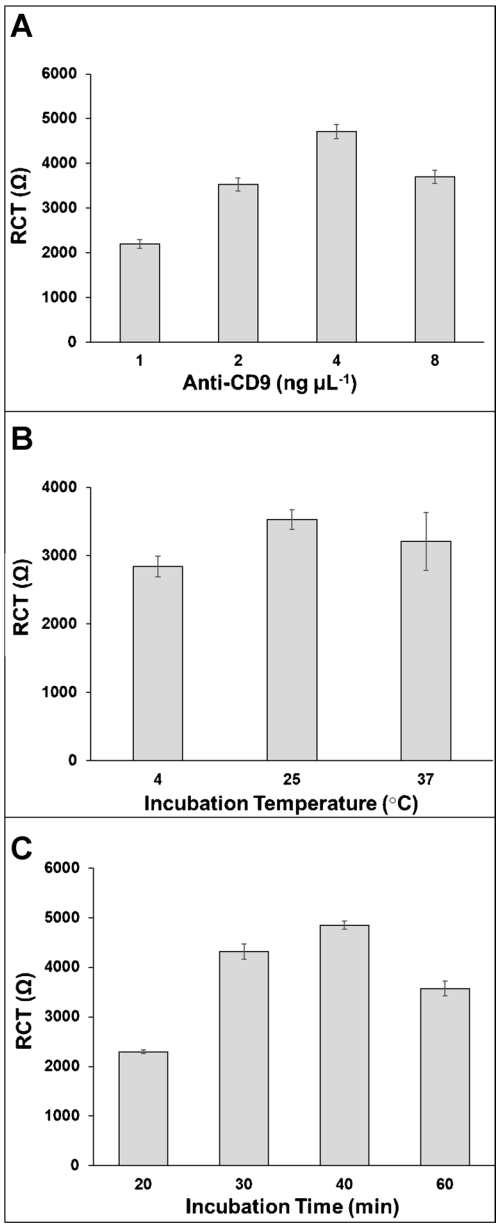


Fig. 4 The effect of Anti-CD9 concentration (**A**), incubation temperature (**B**), and incubation time (**C**) on RCT of 1.0×10^{12} exosomes mL^{-1}

the optimization studies are presented in Figures S5, S6, and S7, respectively.

Analytical performance of biosensors

Working conditions were optimized for the exosome determination, and the analytical performance of the produced exosome biosensor was investigated under these conditions. Figure 5 shows the principle of the exosome biosensor prepared with paper electrodes. After the processes mentioned in Sect. "Fabrication of paper-based electrodes", gold particles were accumulated on carbon WE, which made the surface more electron conductive. The AuPs@PE revealed a small semicircle domain, implying low electron-transfer resistance of the redox probe ($Fe(CN)_6^{3-}/Fe(CN)_6^{4-}$). AuPs@PE exhibited a significant increase in both anodic and cathodic peak currents of the redox probe. Then, Anti-CD9 was conjugated to the surface of AuPs@PE by activating 11-MUA with EDC/NHS coupling agents. Anti-CD9 immobilization reduced the ability of the redox probe to access the layer, and this was characterized by an increase in the RCT values that means the passivation of the electrode. This behavior was also used to obtain a calibration curve for exosome detection between 1×10^5 and 1×10^{12} exosomes mL^{-1}. Lyophilized PC-3 (human metastatic prostate cancer cell line) exosome standards were used to ensure the analytical validity of the method. To assess the immune complex formed by anti-CD9 and CD9 antigen, exosome concentrations ranging from1×10^5 to 1×10^{12} exosomes mL^{-1} in PBS (pH 7.4) were tested by EIS in faradaic conditions. The impedimetric responses of Anti-CD9/AuPs@PE against exosome concentration from seven independently prepared batches are shown in Fig. 6A. The RCT response of exosomes with their increasing concentrations was evaluated, and the calibration curve in Fig. 6B was obtained. The RCT corresponding to each concentration in the calibration curve was obtained by averaging three measurements. According to this curve, a linear variation was established with RCT over an exosome concentration range of 1×10^5 to 1×10^{12} mL^{-1}. The equation $y = 799.66x—598.2$ was obtained for this linearity with 0.9921 of R^2. In addition, the limit of detection (LOD) was obtained to be 8.7×10^2 exosomes mL^{-1}. The examination of Tables S3 and S4 focused on the summary output of the regression statistics and the limit of detection (LOD). In addition, the studies in the literature in which exosome sensors were developed using different methods are indicated in Table 1. Compared to these exosome sensors in the literature, the proposed Anti-CD9/AuPs@PE exhibits a wide linear working range and high sensitivity.

Selectivity, repeatability, and stability of Anti-CD9/AuPs@PE

To verify the selectivity of the proposed sensor for exosome detection, we evaluated the response of Anti-CD9/AuPs@PE to biomolecules present in plasma such as glucose, cysteine, and threonine at concentrations 1 mg mL^{-1}, 0.03 mg mL^{-1}, and 0.03 mg mL^{-1}, respectively. In addition, we used carcinoembryonic antigen (CEA) in the selectivity study. CEA is a glycoprotein abnormally expressed in many cancer types (such as breast cancer, gastric cancer, and ovarian cancer) [64, 65] and the normal range is 0 to 2.5 ng mL^{-1} in blood [66, 67]. In this part, a 2 ng mL^{-1}

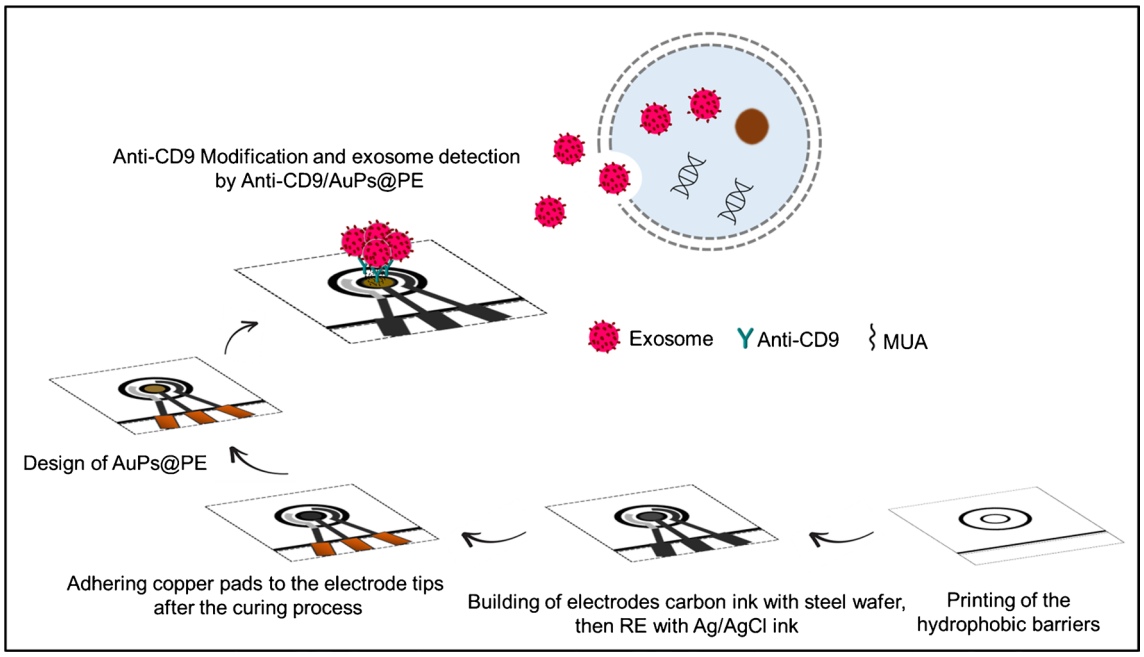


Fig. 5 Design and components of Anti-CD9/AuPs@PE

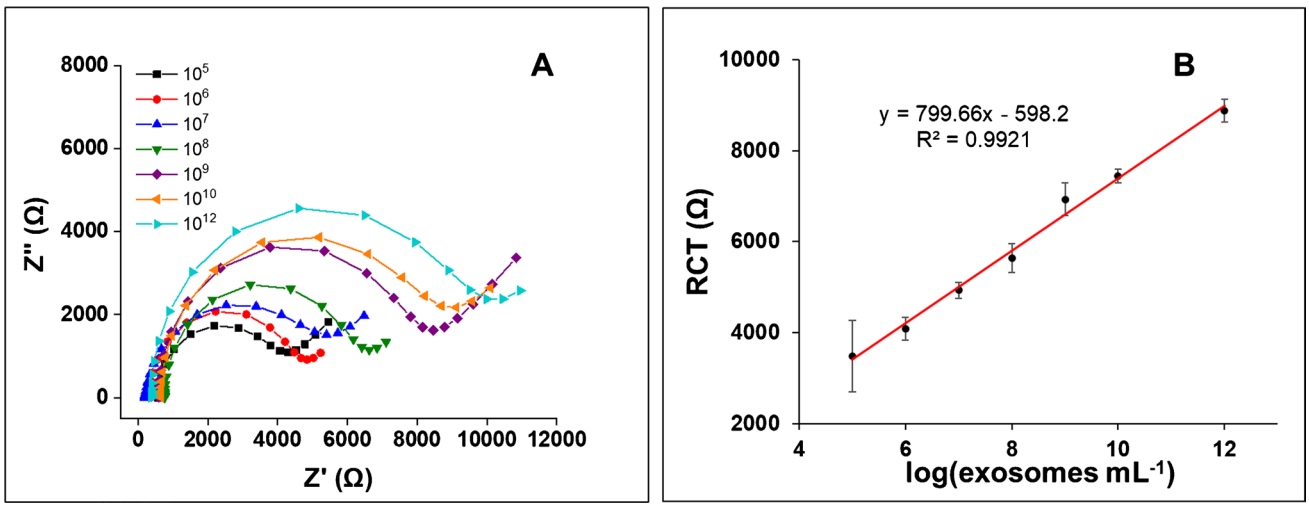


Fig. 6 Calibration curve of linear RCT responses against different exosome concentrations

CEA sample was used to prove the sensor performance. Selectivity testing was performed on the AuPs@PE surface by applying MUA, followed by Anti-CD9, 1% BSA, and the specified biomolecules. We obtained RCT values for glucose, CEA, cysteine, and threonine as 3766.7 ± 22.7 Ω, 3904.3 ± 234.9 Ω, 3983.3 ± Ω 234.3, and 3845.0 ± 84.6 Ω, respectively. The RCT value for Anti-CD9/AuPs@PE and Exo/Anti-CD9/AuPs@PE (1×10^{12} particles mL^{-1}) was obtained as 3650.3 ± 353.8 Ω and 8884.0 ± 248.0 Ω, respectively. We observed that the surface had a low affinity for these biomolecules compared to Anti-CD9/AuPs@PE and Exo/Anti-CD9/AuPs@PE. Figure 7 and Figure S8 reveal that this exosome biosensor displays excellent selectivity. Moreover, the RCT and standard deviation values of the selectivity study and the calculation of relative responses (RR) are given in Table S5 and Table S6, respectively. A low affinity with CEA resulting from protein–protein interaction with the receptor on the sensor surface was observed [68–70]. On the other hand, moving away of gold nanoparticles on the AuNPs@PE may form a bare carbon surface, which may result in the adsorption of CEA antigen to the surface. Such a situation can be predicted as another

Table 1 Comparison of the analytical performance of exosome assays

Technique	Detection range	LOD	Ref
Impedimetric	10^2–10^9 EVs mL^{-1}	77 EVs mL^{-1}	[55]
Colorimetric	10^2 –10^8 particles mL^{-1}	1×10^2 particles mL^{-1}	[56]
Electrical	10^3–10^8 particles mL^{-1}	3×10^2 particles mL^{-1}	[57]
Surface-enhanced Raman spectroscopy	5.44×10^2—2.72×10^4 particles mL^{-1}	5.44×10^2 particles mL^{-1}	[58]
Differential pulse voltammetry	7.61×10^4—7.61×10^8	4.39×10^3 particles mL^{-1}	[59]
Localized surface plasmon resonance	7×10^2- 8.8×10^7 particles mL^{-1}	7×10^2 particles mL^{-1}	[60]
Electrochemical	10^6—10^{10} particles mL^{-1}	2.09×10^4 particles mL^{-1}	[61]
Impedimetric	50×10^{-12} – 200×10^{-9} M	1.9×10^5 particles mL^{-1}	[62]
UV	0.4×10^8—6.0×10^8 particles mL^{-1}	3.58×10^6 particles mL^{-1}	[63]
Impedimetric	2.9×10^3—1.0×10^{12} particles mL^{-1}	8.7×10^2 particles mL^{-1}	Our work

reason for the increase in RCT with the incubation of CEA. In addition, the affinity of cysteine to a gold-plated surface increased the RCT on the surface with chemical binding as shown in Figure S9. To prove that the interaction here is due to -SH groups in cysteine, we performed a selectivity study with threonine which has a similar molecular structure but does not contain an -SH group. In the existence of threonine, Anti-CD9/AuPs@PE showed a lower affinity than the one of cysteine. As a result, the response obtained from other proteins and biomolecules is too low to affect the selectivity of the developed exosome biosensor.

The developed method's intra-day and inter-day accuracy and precision were determined by analyzing exosomes at three different concentrations as 1.0×10^7, 1.0×10^8, and 1.0×10^{10} particles mL^{-1}, respectively. Intraday analyses were performed by analyzing three exosome samples on the same day. The inter-day analysis is the average of four measurements taken at the same concentrations and by the equipment carried on day 1, day 5, day 14, and day 28 for examining one month's performance. Results expressed as relative standard deviation (RSD) for precision are shown in Table 2 for both intraday and intraday values. The relative standard deviations of the EIS results (%RSD < 10%) indicate the reproducibility for both intraday and interday groups $n=3$ and $n=4$, respectively.

Stability is another important parameter that affects the practicality of the proposed biosensor. The aging or destabilization of a biosensor imposes limitations for general use. The long-term stability in vitro of Anti-CD9/AuPs@PE stored at 4 °C was evaluated by measuring the impedance response towards 1.0×10^{10} exosomes mL^{-1} for every day. As shown in Fig. 8A, the impedimetric responses of Anti-CD9/AuPs@PE for the first 14 days were fairly close. Stability responses were also calculated as relative activity % to better explain the surface

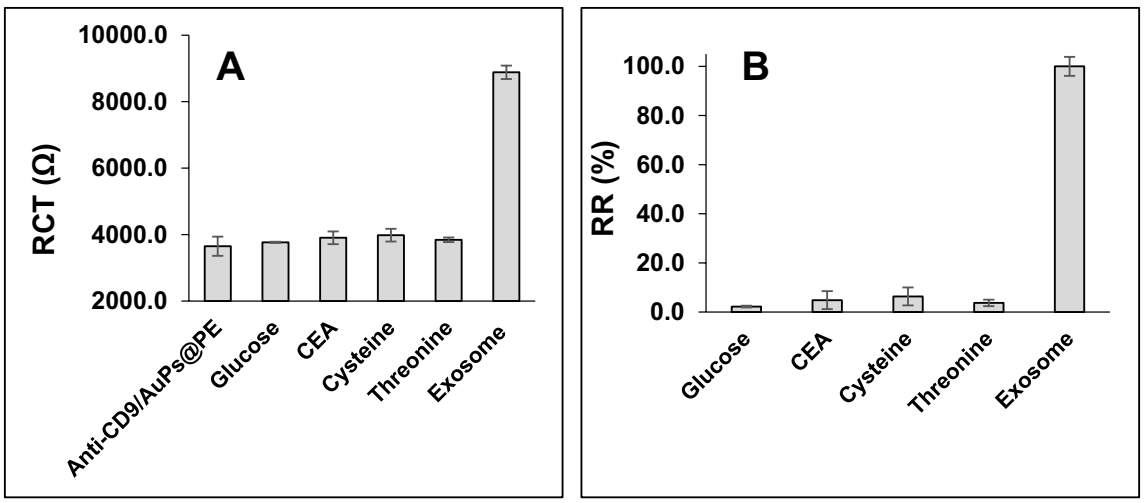


Fig. 7 – The selectivity study of Anti-CD9/AuPs@PE biosensor against CEA (2 ng mL^{-1}), glucose (1 mg mL^{-1}), cysteine (0.03 mg mL^{-1}), threonine (0.03 mg mL^{-1}), and 1×10^{12} particles mL^{-1} standard exosomes (**A**) and relative response studies of each biomolecule (**B**)

Table 2 Intra-day and inter-day reproducibilities of Anti-CD9/AuPs@PE

	Intraday ($n=3$)		Interday ($n=4$)	
Exosome (Log) (particles mL^{-1})	Exosome found (Log) (particles mL^{-1})	%RSD	Exosome found (Log) (particles mL^{-1})	%RSD
7	6.80 ± 0.36	5.29	6.82 ± 0.39	5.72
8	7.79 ± 0.14	1.80	7.66 ± 0.46	6.01
10	10.10 ± 0.53	5.25	9.81 ± 0.43	4.38

Table 3 Recovery data of urine samples from different patients

Sample	Counted concentration (particles mL^{-1})	RCT (Ω)	Found concentration (particles mL^{-1})	Recoveries (%)
G1P1	2.4×10^{6}	4423 ± 42	1.9×10^{6}	79
G1P2	1.0×10^{6}	4161 ± 103	8.9×10^{5}	89
G2P2	3.0×10^{7}	5416 ± 281	3.3×10^{7}	110
G3P1	1.6×10^{8}	5979 ± 406	1.7×10^{8}	106
G3P2	1.4×10^{8}	5863 ± 501	1.2×10^{8}	85

efficiency of the proposed sensor. By the end of work, the relative activity value had dropped to 75%. This may be due to slight degradation of the protein after prolonged storage at 4 °C (Fig. 8B). Nyquist diagram for the stability study of the biosensor is shown in Figure S10. This behavior is within acceptable limits, although instability of 25 percent was detected for the proposed sensor.

Real-life sample analysis of the PE platform

After the validation works, the proposed sensor was tested on urine samples collected from the patients to verify its use in real samples, and the results are listed in Table 3. The analytical performance of the proposed sensor was evaluated with the samples obtained from different patients containing different concentrations of exosomes. We collected urine samples from five patients. In real sample analysis, two patient samples from Group I, which consists of patients who do not have a prostate problem and applied to the clinic due to urinary problem; one patient sample from Group II, which consists of patients who were diagnosed with prostatitis; and two samples from Group III, which consists of patients who were diagnosed with prostate cancer for the first time but were not treated were used. We obtained the number of exosomes after their isolation procedure from each urine sample with ELISA (EXEL-ULTRA-CD63-1, System Biosciences). We applied the impedimetric measurements to the urine samples with Anti-CD9/AuPs@PE by the same procedure. After the evolution of the results, it was seen that the number of exosomes per mL increased because the pathological conditions of the patients progressed from simple urinary problems to cancer. This is explained by the large number of exosomes produced by the high activity of the cancer cells [71, 72]. Briefly, in this part of the study, the exosome concentrations for the patients who have urinary and infection problems and were diagnosed with prostate cancer, along with their acceptable recoveries of the measurements, were evaluated. The proposed Anti-CD9/AuPs@PE demonstrated its potential as a label-free detection tool for cancer diagnosis, capable of discriminating exosome levels in cancer patients.

Conclusions

To summarize, we have developed a functionalized and low-cost paper-based biosensor using AuPs and conjugated anti-CD9 antibodies for the impedimetric and label-free

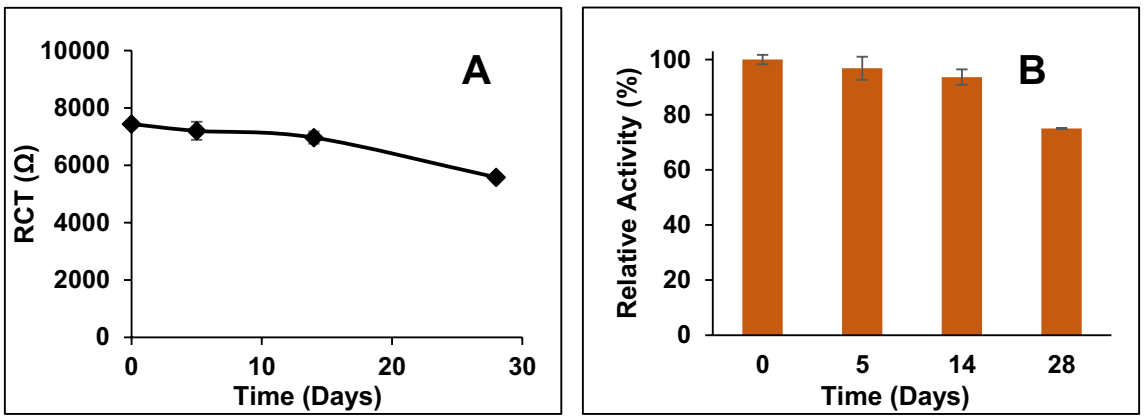


Fig. 8 Stability (**A**) and relative activity (**B**) of Anti-CD9/AuPs@PE sensors stored at + 4 °C for 1 month

detection of exosomes with high sensitivity and specificity. The accumulation of AuPs on the carbon surface provided a great advantage for sensitive measurements due to increased surface area and electrochemical signal quality. The developed paper-based exosome biosensor has the stated advantages as (i) the detection method is directly applicable to urine samples and does not need a label compared to other methods, (ii) LOD value was found to be 8.7×10^2 exosome mL^{-1} with higher precision than many methods in the literature, (iii) it can distinguish the levels of exosomes for the patients having urinary problems. Ultimately, this production method provided a novel, fast, and reliable sensor platform for exosome detection. In addition, the designed system works with only 5.0 µL samples. Analytically, the proposed sensor as a lab-on-paper device can detect the exosomes at ultra-low concentrations in both the buffer solution and urine samples.

Supplementary Information The online version contains supplementary material available at https://doi.org/10.1007/s00604-024-06644-2.

Acknowledgements The authors are thankful to Gazi University Scientific Research Office (FCD-2021-7119). This study originated from a section of Sevda Akay Sazaklioglu's Ph.D. thesis.

Author contribution Sevda Akay Sazaklioglu data curation, investigation, methodology, writing of the original draft, and validation. Hilal Torul investigation, methodology, and formal analysis. Uğur Tamer conceptualization, methodology, and supervision. Hilal Kabadayi Ensarioglu data curation and investigation. Hafize Seda Vatansever resources and methodology. Bilal H. Gumus resources and methodology. Hüseyin Çelikkan conceptualization, methodology, supervision, funding acquisition, review & editing of the manuscript.

Data availability No datasets were generated or analysed during the current study.

Declarations

Ethics approval The urine samples used in this Project were collected with the collaboration work of Manisa Celal Bayar University Faculty of Medicine Department of Urology and Manisa Celal Bayar University Faculty of Medicine, Department of Histology and Embryology with the approval of Manisa Celal Bayar University Faculty of Medicine Health Sciences Ethics Committee dated 25/10/2017 and numbered 20.478.486–164.

Conflict of interest The authors declare no competing interests.

References

1. Fitzmaurice C, Dicker D, Pain A et al (2015) The Global Burden of Cancer 2013. JAMA Oncol 1:505–527. https://doi.org/10.1001/jamaoncol.2015.0735
2. Sidorova EA, Zhernov Y, v., Antsupova MA, et al (2023) The role of different types of microRNA in the pathogenesis of breast and prostate cancer. Int J Mol Sci 24:1980. https://doi.org/10.3390/ijms24031980
3. Aprile M, Costa V, Cimmino A, Calin GA (2022) Emerging role of oncogenic long noncoding RNA as cancer biomarkers. Int J Cancer 152:822–834
4. Becker A, Thakur BK, Weiss JM et al (2016) Extracellular vesicles in cancer: cell-to-cell mediators of metastasis. Cancer Cell 30:836–848
5. Keller S, König AK, Marmé F et al (2009) Systemic presence and tumor-growth promoting effect of ovarian carcinoma released exosomes. Cancer Lett 278:73–81. https://doi.org/10.1016/j.canlet.2008.12.028
6. Le MTN, Hamar P, Guo C et al (2014) MiR-200-containing extracellular vesicles promote breast cancer cell metastasis. J Clin Investig 124:5109–5128. https://doi.org/10.1172/JCI75695
7. Melo SA, Luecke LB, Kahlert C et al (2015) Glypican-1 identifies cancer exosomes and detects early pancreatic cancer. Nature 523:177–182. https://doi.org/10.1038/nature14581
8. Liu X, Lu Y, Xu Y et al (2019) Exosomal transfer of miR-501 confers doxorubicin resistance and tumorigenesis via targeting of BLID in gastric cancer. Cancer Lett 459:122–134. https://doi.org/10.1016/j.canlet.2019.05.035
9. Khan S, Bennit HF, Turay D, et al (2014) Early diagnostic value of surviving and its alternative splice variants in breast cancer. BMC Cancer 14:. https://doi.org/10.1186/1471-2407-14-176
10. Taylor DD, Gercel-Taylor C (2008) MicroRNA signatures of tumor-derived exosomes as diagnostic biomarkers of ovarian cancer. Gynecol Oncol 110:13–21. https://doi.org/10.1016/j.ygyno.2008.04.033
11. Riches A, Campbell E, Borger E, Powis S (2014) Regulation of exosome release from mammary epithelial and breast cancer cells-a new regulatory pathway. Eur J Cancer 50:1025–1034. https://doi.org/10.1016/j.ejca.2013.12.019
12. Kim B, Kim K-M (2023) Role of exosomes and their potential as biomarkers in Epstein-Barr virus-associated gastric cancer. Cancers (Basel) 15:469. https://doi.org/10.3390/cancers15020469
13. Bamankar S, Londhe VY (2023) The rise of extracellular vesicles as new age biomarkers in cancer diagnosis: promises and pitfalls. Technol Cancer Res Treat 22 https://doi.org/10.1177/15330338221149266
14. Zhou Y, Chi H, Wu Y et al (2016) Organic additives stabilize RNA aptamer binding of malachite green. Talanta 160:172–182. https://doi.org/10.1016/j.talanta.2016.06.067
15. Chen J, Meng HM, An Y, et al (2020) Structure-switching aptamer triggering hybridization displacement reaction for label-free detection of exosomes. Talanta 209:. https://doi.org/10.1016/j.talanta.2019.120510
16. Zheng XS, Jahn IJ, Weber K et al (2018) Label-free SERS in biological and biomedical applications: recent progress, current challenges and opportunities. Spectrochim Acta A Mol Biomol Spectrosc 197:56–77. https://doi.org/10.1016/j.saa.2018.01.063
17. Wang Q, Zou L, Yang X et al (2019) Direct quantification of cancerous exosomes via surface plasmon resonance with dual gold nanoparticle-assisted signal amplification. Biosens Bioelectron 135:129–136. https://doi.org/10.1016/j.bios.2019.04.013
18. Zhang J, Wang LL, Hou MF et al (2018) A ratiometric electrochemical biosensor for the exosomal microRNAs detection based on bipedal DNA walkers propelled by locked nucleic acid modified toehold mediate strand displacement reaction. Biosens Bioelectron 102:33–40. https://doi.org/10.1016/j.bios.2017.10.050
19. Taylor DD, Gercel-Taylor C (2011) Exosomes/microvesicles: mediators of cancer-associated immunosuppressive microenvironments. Semin Immunopathol 33:441–454
20. Seipold L, Saftig P (2016) The emerging role of tetraspanins in the proteolytic processing of the amyloid precursor protein. Front Mol Neurosci 9:. https://doi.org/10.3389/fnmol.2016.00149

21. Brosseau C, Colas L, Magnan A, Brouard S (2018) CD9 tetraspanin: a new pathway for the regulation of inflammation? Front Immunol 9:2316
22. Khushman M, Bhardwaj A, Patel GK, et al (2017) Exosomal markers (CD63 and CD9) expression pattern using immunohistochemistry in resected malignant and nonmalignant pancreatic specimens. In: Pancreas. Lippincott Williams and Wilkins, pp 782–788
23. Grønborg M, Kristiansen TZ, Iwahori A et al (2006) Biomarker discovery from pancreatic cancer secretome using a differential proteomic approach. Mol Cell Proteomics 5:157–171
24. An J, Park H, Kim J et al (2023) Extended-gate field-effect transistor consisted of a CD9 aptamer and MXene for exosome detection in human serum. ACS Sens 8:3174–3186. https://doi.org/10.1021/acssensors.3c00879
25. Doldán X, Fagúndez P, Cayota A et al (2016) Electrochemical sandwich immunosensor for determination of exosomes based on surface marker-mediated signal amplification. Anal Chem 88:10466–10473. https://doi.org/10.1021/acs.analchem.6b02421
26. Sazaklıoğlu SA, Torul H, Vatansever HS et al (2022) Direct impedimetric detection of exosomes and practical application in urine. J Appl Electrochem. https://doi.org/10.1007/s10800-022-01753-3
27. Dutta G (2022) Electrochemical detection of cancer fingerprint: a systematic review on recent progress in extracellular vesicle research from lab to market. In: Next-Generation Nanobiosensor Devices for Point-Of-Care Diagnostics. Springer Nature. https://doi.org/10.1007/978-981-19-7130-3_3
28. Pandey N, Mandal M, Samanta D, et al (2023) A nanobody based ultrasensitive electrochemical biosensor for the detection of soluble CTLA-4 –A candidate biomarker for cancer development and progression. Biosens Bioelectron 242:. https://doi.org/10.1016/j.bios.2023.115733
29. Lazanas AC, Prodromidis MI (2023) Electrochemical impedance spectroscopy—a tutorial. ACS Measurement Science Au 3:162–193
30. Pradhan R, Kalkal A, Jindal S et al (2020) Four electrode-based impedimetric biosensors for evaluating cytotoxicity of tamoxifen on cervical cancer cells. RSC Adv 11:798–806. https://doi.org/10.1039/d0ra09155c
31. Uygun ZO, Yeniay L, GïrgïnSağın F, (2020) CRISPR-dCas9 powered impedimetric biosensor for label-free detection of circulating tumor DNAs. Anal Chim Acta 1121:35–41. https://doi.org/10.1016/j.aca.2020.04.009
32. Xie Q-Z, Lin M-W, Hsu W-E, Lin C-T (2020) Review—advancements of nanoscale structures and materials in impedimetric biosensing technologies. ECS J Solid State Sci Technol 9:115027. https://doi.org/10.1149/2162-8777/abbcb3
33. Kirchhain A, Bonini A, Vivaldi F et al (2020) Latest developments in non-faradic impedimetric biosensors: towards clinical applications. TrAC - Trends in Anal Chem 133:116073
34. Dutta G, Rainbow J, Zupancic U et al (2018) Microfluidic devices for label-free DNA detection. Chemosensors 6:43
35. Diaz-Armas GG, Cervantes-Gonzalez AP, Martinez-Duarte R, Perez-Gonzalez VH (2022) Electrically driven microfluidic platforms for exosome manipulation and characterization. Electrophoresis 43:327–339
36. Prodromidis MI (2010) Impedimetric immunosensors-a review. Electrochim Acta 55:4227–4233
37. Dutta G, Jallow AA, Paul D, Moschou D (2019) Label-free electrochemical detection of S. mutans exploiting commercially fabricated printed circuit board sensing electrodes. Micromachines (Basel) 10:. https://doi.org/10.3390/mi10090575
38. Ming T, Luo J, Liu J et al (2020) Paper-based microfluidic aptasensors. Biosens Bioelectron 170:112649
39. Yarali E, Eksin E, Torul H, et al (2022) Impedimetric detection of miRNA biomarkers using paper-based electrodes modified with bulk crystals or nanosheets of molybdenum disulfide. Talanta 241:. https://doi.org/10.1016/j.talanta.2022.123233
40. Ozer T, Henry CS (2021) Paper-based analytical devices for virus detection: recent strategies for current and future pandemics. TrAC-Trends Anal Chem 144:116424
41. Liu S, Su W, Ding X (2016) A review on microfluidic paper-based analytical devices for glucose detection. Sensors (Switzerland) 16:1–17
42 Pang R, Zhu Q, Wei J et al (2022) Enhancement of the detection performance of paper-based analytical devices by nanomaterials. Molecules 27:508
43. Wang P, Kricka LJ (2018) Current and emerging trends in point-of-care technology and strategies for clinical validation and implementation. Clin Chem 64:1439–1452
44. Biswas P, Mukherjee A, Goyal P, et al (2024) A rapid diagnostic technology for isolating rare blood group patients under medical emergency using a three-fold paper-polymer microfluidic kit. Sens Actuators B Chem 409:. https://doi.org/10.1016/j.snb.2024.135650
45. St John A, Price CP point-of-care testing technologies Clin Biochem Rev 35 (3) 2014 155 Existing and Emerging Technologies for Point-of-Care Testing
46. Yetisen AK, Akram MS, Lowe CR (2013) Paper-based microfluidic point-of-care diagnostic devices. Lab Chip 13:2210–2251
47. Sazaklioglu SA, Torul H, Kabadayi H et al (2022) Calibration curve approaches for nonlinear data points obtained in Colo 320 exosomes determination. Anal Bioanal Electrochem 14(11):1027–43
48. Wongkaew N, Simsek M, Griesche C, Baeumner AJ (2019) Functional nanomaterials and nanostructures enhancing electrochemical biosensors and lab-on-a-chip performances: recent progress, applications, and future perspective. Chem Rev 119:120–194
49. Collinson MM (2013) Nanoporous gold electrodes and their applications in analytical chemistry. ISRN Anal Chem 2013:1–21. https://doi.org/10.1155/2013/692484
50. Eksin E, Torul H, Yarali E, et al (2021) Paper-based electrode assemble for impedimetric detection of miRNA. Talanta 225:. https://doi.org/10.1016/j.talanta.2020.122043
51. Yu Y, Li YT, Jin D et al (2019) Electrical and label-free quantification of exosomes with a reduced graphene oxide field effect transistor biosensor. Anal Chem 91:10679–10686. https://doi.org/10.1021/acs.analchem.9b01950
52. Pan S, Pei L, Zhang A, et al (2020) Passion fruit-like exosome-PMA/Au-BSA@Ce6 nanovehicles for real-time fluorescence imaging and enhanced targeted photodynamic therapy with deep penetration and superior retention behavior in tumor. Biomaterials 230 https://doi.org/10.1016/j.biomaterials.2019.119606
53. Rafighdoust Z, Baharara J, Forghanifard MM, Kerachian MA (2021) Isolation and characterization of exosomes derived from breast cancer MDA-MB-231 cell line. Gene Cell Tissue 8 https://doi.org/10.5812/gct.110505
54. Kore RA, Henson JC, Hamzah RN, et al (2019) Molecular events in MSC exosome mediated cytoprotection in cardiomyocytes. Sci Rep 9 https://doi.org/10.1038/s41598-019-55694-7
55. Kilic T, Valinhas ATDS, Wall I, et al (2018) Label-free detection of hypoxia-induced extracellular vesicle secretion from MCF-7 cells. Sci Rep 8 https://doi.org/10.1038/s41598-018-27203-9
56. Liu W, Li J, Wu Y et al (2018) Target-induced proximity ligation triggers recombinase polymerase amplification and transcription-mediated amplification to detect tumor-derived exosomes in nasopharyngeal carcinoma with high sensitivity. Biosens Bioelectron 102:204–210. https://doi.org/10.1016/j.bios.2017.11.033

57. Gu C, Bai L, Pu L, et al (2021) Highly sensitive and stable self-powered biosensing for exosomes based on dual metal-organic frameworks nanocarriers. Biosens Bioelectron 176 https://doi.org/10.1016/j.bios.2020.112907
58. da Li T, Zhang R, Chen H et al (2018) An ultrasensitive polydopamine bi-functionalized SERS immunoassay for exosome-based diagnosis and classification of pancreatic cancer. Chem Sci 9:5372–5382. https://doi.org/10.1039/c8sc01611a
59. Xu H, Liao C, Zuo P et al (2018) Magnetic-based microfluidic device for on-chip isolation and detection of tumor-derived exosomes. Anal Chem 90:13451–13458. https://doi.org/10.1021/acs.analchem.8b03272
60. Liu L, Thakur A, Kar Li W, et al (2022) Site specific biotinylated antibody functionalized Ag@AuNIs LSPR biosensor for the ultrasensitive detection of exosomal MCT4, a glioblastoma progression biomarker. Chem Eng J 446 https://doi.org/10.1016/j.cej.2022.137383
61. Wang S, Zhang L, Wan S et al (2017) Aptasensor with expanded nucleotide using DNA nanotetrahedra for electrochemical detection of cancerous exosomes. ACS Nano 11:3943–3949. https://doi.org/10.1021/acsnano.7b00373
62. Li Q, Tofaris GK, Davis JJ (2017) Concentration-normalized electroanalytical assaying of exosomal markers. Anal Chem 89:3184–3190. https://doi.org/10.1021/acs.analchem.6b05037
63. Chen J, Xu Y, Lu Y, Xing W (2018) Isolation and visible detection of tumor-derived exosomes from plasma. Anal Chem 90:14207–14215. https://doi.org/10.1021/acs.analchem.8b03031
64. Joshi S, Raj KA, Rao MR, Ghosh R (2022) An electronic biosensor based on semiconducting tetrazine polymer immobilizing matrix coated on rGO for carcinoembryonic antigen. Sci Rep 12 https://doi.org/10.1038/s41598-022-06976-0
65. Suan Ng S, Ling Lee H, Bothi Raja P, Doong R an (2022) Recent advances in nanomaterial-based optical biosensors as potential point-of-care testing (PoCT) probes in carcinoembryonic antigen detection. Chem Asian J https://doi.org/10.1002/asia.202200287
66. Li J, Liu L, Ai Y et al (2020) Self-polymerized dopamine-decorated Au NPs and coordinated with Fe-MOF as a dual binding sites and dual signal-amplifying electrochemical aptasensor for the detection of CEA. ACS Appl Mater Interfaces 12:5500–5510. https://doi.org/10.1021/acsami.9b19161
67. Moreno García V, Cejas P, Blanco Codesido M et al (2009) Prognostic value of carcinoembryonic antigen level in rectal cancer treated with neoadjuvant chemoradiotherapy. Int J Colorectal Dis 24:741–748. https://doi.org/10.1007/s00384-009-0682-6
68. Snider J, Kotlyar M, Saraon P, et al (2015) Fundamentals of protein interaction network mapping. Mol Syst Biol 11:848 https://doi.org/10.15252/msb.20156351
69. Soltermann F, Struwe WB, Kukura P (2021) Label-free methods for optical: In vitro characterization of protein-protein interactions. Phys Chem Chem Phys 23:16488–16500. https://doi.org/10.1039/d1cp01072g
70. Roth S, Zander I, Michelson Y, et al (2020) Identification of protein-protein interactions using a magnetic modulation biosensing system. Sens Actuators B Chem 303:. https://doi.org/10.1016/j.snb.2019.127228
71. Lorencova L, Bertok T, Bertokova A et al (2020) Exosomes as a source of cancer biomarkers: advances in electrochemical biosensing of exosomes. ChemElectroChem 7:1956–1973
72. Tutanov O, Proskura K, Kamyshinsky R, et al (2020) Proteomic profiling of plasma and total blood exosomes in breast cancer: a potential role in tumor progression, diagnosis, and prognosis. Front Oncol 10:. https://doi.org/10.3389/fonc.2020.580891

Publisher's Note Springer Nature remains neutral with regard to jurisdictional claims in published maps and institutional affiliations.

Springer Nature or its licensor (e.g. a society or other partner) holds exclusive rights to this article under a publishing agreement with the author(s) or other rightsholder(s); author self-archiving of the accepted manuscript version of this article is solely governed by the terms of such publishing agreement and applicable law.